Computer Analysis of Short-Boundary Planar Circuits

TAKANORI OKOSHI, MEMBER, IEEE, AND SEIKO KITAZAWA

Abstract—**A method of computer analysis of planar (two-dimensional) circuits having an arbitrarily shaped short boundary is proposed. The proposed method is based upon the contour integral representation of the two-dimensional wave equation. Results of the computer analyses for simple circuits are compared with analytical solutions to show the validity and accuracy of the proposed method. Some examples of analyses of practical circuits are also presented.**

I. INTRODUCTION

THE planar circuit is a circuit concept proposed by one of the authors in 1969. It is the two-dimensional circuit that should be positioned between the distributed-constant (one-dimensional) circuit and the waveguide (three-dimensional) circuit; it is defined as an electrical circuit having dimensions comparable to the wavelength in two directions but much less thickness in one direction. The planar circuit can be classified into three types: the triplate type, open (or asymmetric) type, and short-boundary type [1].

In the past five years, the authors and their co-workers in Japan have been concentrating principally upon the analysis and design of the triplate-type planar circuits, which have open-circuit boundaries. It was because the investigation of the triplate type seemed most urgent in connection with the development of the microwave IC technology.

This paper proposes a method of the computer analysis of an arbitrarily shaped, short-boundary planar circuit. Some examples of analyses of practical circuits are also presented.

The computer-analysis technique described in this paper enables us to know the precise characteristics of circuits such as are shown in Fig. 1(a)–(c). Moreover, in the case of Fig. 1(b), the height of the waveguide need not be small compared to the wavelength as required by the definition of the planar circuit; the present analysis can also be applied to the ordinary TE_{10}-mode waveguide circuitry provided that no transverse electric field is present. Therefore the advantages of the computer-analysis technique of the short-boundary-type planar circuit extend to the conventional waveguide technology.

II. PRINCIPLE OF ANALYSIS

The computer-analysis technique developed for the triplate type may be modified to its "dual" form for its application to the short-boundary type. The most important change stems from the fact that the coupling ports

Manuscript received May 6, 1974; revised July 25, 1974.
The authors are with the Department of Electronic Engineering, University of Tokyo, Tokyo Japan.

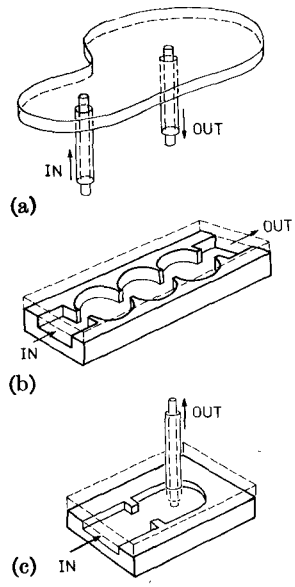

Fig. 1. Examples of the short-boundary planar circuit. (a) Coaxial-coupled type. (b) Waveguide-coupled type. (c) Mixed type.

are of entirely different form. For example, when a planar circuit is coupled to the external circuits through waveguides as shown in Fig. 1(b), a computational process is required to provide the "match" between the electromagnetic field in the planar circuit and the proper fields in the waveguides at properly selected reference planes. The coaxial ports as shown in Fig. 1(a) and (c) also require a similar computational process. In any case, the basic equation for the open-boundary planar circuit can be utilized in the earlier stage of the following analysis.

In [1], it was shown that by using Weber's solution of the two-dimensional wave equation [2], the RF voltage at a point upon the periphery of an arbitrarily shaped, homogeneous two-dimensional wave medium is given as

$$2jV(s) = \oint_c [k \cos\theta H_1^{(2)}(kr) V(s_0) - j\omega\mu d\, H_0^{(2)}(kr) i_n(s_0)]\, ds_0. \quad (1)$$

In this equation, $H_0^{(2)}$ and $H_1^{(2)}$ are the zeroth-order and first-order Hankel functions of the second kind, respectively, i_n denotes the current density flowing outwards along the periphery, s and s_0 denote the distance along the periphery C. The variable r denotes distance between points (s) and (s_0), and θ denotes the angle made by the straight line from point (s) to point (s_0) and the normal at point (s_0), as shown in Fig. 2. When i_n is given, (1) is a second-kind Fredholm integral equation with respect to the RF voltage V.

To avoid useless confusions, we restrict the following

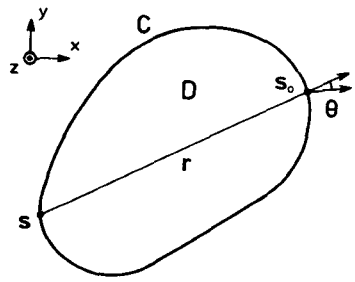

Fig. 2. Symbols used in the basic equation.

discussion to two cases. The first case is the short-boundary planar circuit having two coaxial coupling ports as shown in Fig. 1(a). The second case is that having two waveguide coupling ports as shown in Fig. 1(b). The description of the latter case will be emphasized for its practical importance. More complicated cases such as that shown in Fig. 1(c) and those circuits having three or more ports will be dealt with by modifying or combining the analyses for the previous two cases.

III. SHORT-BOUNDARY PLANAR CIRCUIT HAVING TWO COAXIAL COUPLING PORTS

A. Basic Equation

For numerical calculation we divide the periphery of a circuit as shown in Fig. 1(a) into M incremental sections, and provide M sampling points at the center of each section as shown in Fig. 3. We assume that current flows uniformly in each section. The peripheries of the coupling conductors are also divided into m and n incremental sections, and sampling points are provided. Those $m + n + M$ sampling points are numbered as follows:

1) conductor 1: $i = 1 \sim m$;
2) conductor 2: $i = (m + 1) \sim (m + n)$;
3) circuit periphery: $i = (m + n + 1) \sim (m + n + M)$.

It was shown in [1] that if we rewrite (1) into an incremental form, we obtain a matrix equation

$$2j\begin{bmatrix} V_1 \\ \cdot \\ \cdot \\ \cdot \\ V_N \end{bmatrix} = k[G_{ij}]\begin{bmatrix} V_1 \\ \cdot \\ \cdot \\ \cdot \\ V_N \end{bmatrix} + j\omega\mu\, d[F_{ij}]\begin{bmatrix} I_1 \\ \cdot \\ \cdot \\ \cdot \\ I_N \end{bmatrix} \tag{2}$$

$$G_{ij} = \begin{cases} \cos\theta_{ij} H_1^{(2)}(kr_{ij})\, W_j, & (i \neq j) \\ 0, & (i = j) \end{cases}$$

$$F_{ij} = \begin{cases} H_0^{(2)}(kr_{ij}), & (i \neq j) \\ 1 - (2j/\pi)[\log(kW_i/4) - 1 + \gamma], & (i = j) \end{cases}$$

where γ denotes Euler's constant ($=0.5772$), W_i, W_j, and $I_i (= -i_n W_i)$ denote the widths of the ports (i and j) and the current flowing into port i, respectively, and $N \triangleq m + n + M$.

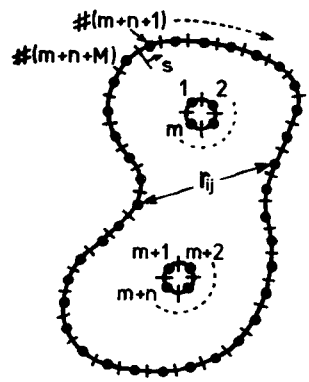

Fig. 3. Symbols used in the computer analysis—I (case of the coaxial-coupled type).

(Equation (1) is derived in [1] for the case in which there is no "hole" in the circuit, in other words when the circuit pattern is singly connected. However, (1) is applicable also to a multiply connected pattern such as is shown in Fig. 3; the proof is given in the Appendix.)

If we further define

$$[U] = 2j[E] - k[G], \qquad (E\text{: unity matrix}) \tag{3}$$

$$[H] = j\omega\mu\, d[F] \tag{4}$$

we obtain, immediately from (1), a simple equation

$$[U_{ij}]\begin{bmatrix} V_1 \\ V_2 \\ \cdot \\ \cdot \\ \cdot \\ V_N \end{bmatrix} = [H_{ij}]\begin{bmatrix} I_1 \\ I_2 \\ \cdot \\ \cdot \\ \cdot \\ I_N \end{bmatrix}. \tag{5}$$

B. Simplification of the Basic Equation

For simplicity we assume the following conditions for the position and size of the coupling conductors.

1) The radius of the conductors R is much less than the wavelength ($R \ll \lambda$, or $kR \ll 1$).

2) If we denote the distance from the center of the conductor to the nearest spot upon the circuit periphery by $r_{\min}$, $R \ll r_{\min}$ holds.

Then we may assume that the voltage V and current density i_n are both uniform along the periphery of the conductor.[1] Therefore, if the voltages and currents of two terminals p and q (see Fig. 3) are denoted by V_p, V_q, I_p, and I_q, respectively, the voltages and currents in each section around the conductors are given as V_p, V_q, I_p/m, and I_q/n. On the other hand, along the circuit periphery $V = 0$ holds. Hence, we may write

[1] We may remove this assumption if we consider $(m - 1)$ and $(n - 1)$ higher order modes in coaxial waveguides 1 and 2, respectively. Then we may take into account the (probably) reactive line impedances for those higher order modes, and we no longer need the reduction of the constraints performed to obtain (7) and (8). A longer computer time will be required, however.

$$[U_{ij}]\begin{bmatrix} V_p \\ \vdots \\ V_p \\ V_q \\ \vdots \\ V_q \\ 0 \\ \vdots \\ 0 \end{bmatrix}\begin{matrix}\} m \\ \\ \\ \} n \\ \\ \\ \} M \\ \\ \end{matrix} = [H_{ij}]\begin{bmatrix} I_p/m \\ \vdots \\ I_p/m \\ I_q/n \\ \vdots \\ I_q/n \\ I_{m+n+1} \\ \vdots \\ I_{m+n+M} \end{bmatrix}\begin{matrix}\} m \\ \\ \\ \} n \\ \\ \\ \} M \\ \\ \end{matrix} . \quad (6)$$

Equation (6) consists of $N(=m+n+M)$ scalar equations, whose number is greater than the number of variables $(M+2)$. To decrease the number of constraints, we define reduced matrices with $(M+2) \times (M+2)$ elements:

$$[U'] = \left[\begin{array}{cc|c} \sum_{i=1}^{m}\sum_{j=1}^{m} U_{ij} & \sum_{i=1}^{m}\sum_{j=m+1}^{m+n} U_{ij} & \sum_{i=1}^{m} U_{i(m+n+1)} \cdots \\ \sum_{i=m+1}^{m+n}\sum_{j=1}^{m} U_{ij} & \sum_{i=m+1}^{m+n}\sum_{j=m+1}^{m+n} U_{ij} & \sum_{i=m+1}^{m+n} U_{i(m+n+1)} \cdots \\ \hline \sum_{j=1}^{m} U_{(m+n+1)j} & \sum_{j=m+1}^{m+n} U_{(m+n+1)j} & U_{m+n+1\,m+n+1} \cdots U_{m+n+M\,m+n+M} \end{array}\right] \quad (7)$$

$$[H'] = \text{(similar to the above)}. \quad (8)$$

Then we may further rewrite (6) as

$$[U']\begin{bmatrix} V_p \\ V_q \\ 0 \\ \vdots \\ 0 \end{bmatrix}\begin{matrix}\} 2 \\ \\ \} M \\ \\ \end{matrix} = [H']\begin{bmatrix} I_p/m \\ I_q/n \\ I_{m+n+1} \\ \vdots \\ I_{m+n+M} \end{bmatrix}\begin{matrix}\} 2 \\ \\ \} M \\ \\ \end{matrix} . \quad (9)$$

The previous simplification implies that "each of the m (or n) sampling points is equally weighted."

C. Derivation of Admittance Parameters

We may derive the admittance parameters Y_{pp}, Y_{pq}, Y_{qp}, and Y_{qq} directly from H' and U'. First, we temporarily consider that all the $(M+2)$ sampling points are coupling terminals and that the planar circuit is represented by an $(M+2)$-port equivalent circuit. The admittance matrix Y of such a circuit is given from (9) as

$$[Y] = [H']^{-1}[U']. \quad (10)$$

The desired parameters Y_{pp}, Y_{pq}, Y_{qp}, and Y_{qq} will be found in the top left corner of the matrix Y. (This method can readily be applied to cases in which the circuit has three or more ports.)

However, practically, the previous computation requires rather long computer time. When the circuit has only two ports, we have a simpler alternative which will be described in the following subsection.

D. Derivation of Transfer Parameters

We assume that the terminals p and q are driving and load terminals, respectively, and impedances Z_p and Z_q are connected to them. Then Z_p must have a negative real part, and must be equal to the driving point impedance multiplied by -1, provided that a stable oscillation exists in the circuit. Since

$$Z_p = -V_p/I_p \quad (11)$$

$$Z_q = -V_q/I_q \quad (12)$$

holds, (9) is rewritten as

$$\{[H'] + mZ_p[X] + nZ_q[W]\}\begin{bmatrix} I_p/m \\ I_q/n \\ I_{m+n+1} \\ \vdots \\ I_{m+n+M} \end{bmatrix} = 0 \quad (13)$$

where X and W are again matrices determined by the shape of the circuit:

$$[X] = \left[\begin{array}{c|c} \overset{1}{U_{11}'} & 0 \cdots 0 \\ U_{21}' & \begin{matrix}\cdot & \cdot \\ \cdot & \cdot \\ \cdot & \cdot\end{matrix} \\ \hline U_{(M+2)1}' & 0 \cdots 0 \end{array}\right] \quad (14a)$$

$$[W] = \left[\begin{array}{c|c|c} 0 & \overset{2}{U_{12}'} & 0 \cdots 0 \\ \cdot & & \begin{matrix}\cdot & \cdot \\ \cdot & \cdot \\ \cdot & \cdot\end{matrix} \\ \cdot & U_{22}' & \\ \cdot & \cdot & \\ \cdot & \cdot & \\ \cdot & \cdot & \\ 0 & U_{(M+2)2}' & 0 \cdots 0 \end{array}\right] . \quad (14b)$$

In order that (13) has a nontrivial solution, i.e., a steady field exists in the circuit,

$$\det [H' + mZ_pX + nZ_qW] = 0 \tag{15}$$

must hold. This equation leads directly to a bilinear relation between $-Z_p$, the driving point impedance, and Z_q, the load impedance, as

$$-Z_p = \frac{A'Z_q + B'}{C'Z_q + D'} \tag{16}$$

where A', B', C', and D' are given as the following determinants

$$A' = n \det \begin{bmatrix} H_{11}' & \overset{2}{U_{12}'} & H_{13}' \cdots H_{1N'}' \\ & & \cdot \quad \cdot \\ H_{21}' & U_{22}' & \cdot \quad \cdot \\ \cdot & \cdot & \cdot \quad \cdot \\ \cdot & \cdot & \cdot \quad \cdot \\ \cdot & \cdot & \cdot \quad \cdot \\ H_{N'1}' & U_{N'2}' & H_{N'3}' \cdots H_{N'N'}' \end{bmatrix} \tag{17a}$$

$$B' = \det [H_{ij}'] \tag{17b}$$

$$C' = mn \det \begin{bmatrix} \overset{1}{U_{11}'} & \overset{2}{U_{12}'} & H_{13}' \cdots H_{1N'}' \\ & & \cdot \quad \cdot \\ U_{21}' & U_{22}' & \cdot \quad \cdot \\ \cdot & \cdot & \cdot \quad \cdot \\ \cdot & \cdot & \cdot \quad \cdot \\ \cdot & \cdot & \cdot \quad \cdot \\ U_{N'1}' & U_{N'2}' & H_{N'3}' \cdots H_{N'N'}' \end{bmatrix} \tag{17c}$$

$$D' = m \det \begin{bmatrix} \overset{1}{U_{11}'} & H_{12}' \cdots H_{1N'}' \\ & \cdot \quad \cdot \\ U_{21}' & \cdot \quad \cdot \\ \cdot & \cdot \quad \cdot \\ \cdot & \cdot \quad \cdot \\ \cdot & \cdot \quad \cdot \\ U_{N'1}' & H_{N'2}' \cdots H_{N'N'}' \end{bmatrix} \tag{17d}$$

where $N' \triangleq M + 2$.

Equation (16) shows that A', B', C', and D' are quantities proportional to the so-called transfer parameters A, B, C, and D of the equivalent two-port circuit. In order that the reciprocity condition ($(AD - BC)^{1/2} = 1$) holds, we should divide A', B', C', and D' by $(A'D' - B'C')^{1/2}$ to get A, B, C, and D, respectively, as

$$\begin{bmatrix} A & B \\ C & D \end{bmatrix} = (A'D' - B'C')^{-1/2} \begin{bmatrix} A' & B' \\ C' & D' \end{bmatrix}. \tag{18}$$

IV. SHORT-BOUNDARY PLANAR CIRCUIT HAVING TWO WAVEGUIDE COUPLING PORTS

A. Basic Equation

We now consider a waveguide-coupled circuit as shown in Fig. 1(b), but having a more arbitrary peripheral shape. The periphery of the circuit is again divided and numbered, as shown in Fig. 4, as follows:

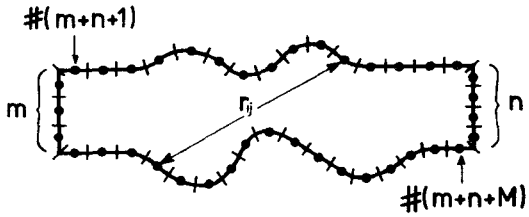

Fig. 4. Symbols used in the computer analysis—II (case of the waveguide-coupled type).

1) input port 1: $i = 1 \sim m$;
2) output port 2: $i = (m + 1) \sim (m + n)$;
3) circuit periphery: $i = (m + n + 1) \sim (m + n + M)$;

and $m + n + M (= N)$ sampling points are provided. The derivation of the $N \times N$ matrix equation (5) follows entirely the same process as was described in the preceding section.

B. Simplification of the Basic Equation

We now assume for simplicity that straight waveguide sections with appropriate length exist on both sides of the input and output planes, so that only the TE_{10}-mode exists at those planes.[2] Under this assumption we may relate $V_1 \sim V_m$ and $I_1 \sim I_m$, $V_{m+1} \sim V_{m+n}$ and $I_{m+1} \sim I_{m+n}$ with simple proportionality formulas. We use representative values of those voltages and currents defined as V_p and V_q: voltages at the center of the input and output reference planes, respectively; and I_p and I_q: currents flowing across the entire widths of the input and output reference planes, respectively. Since the variation of the voltage and current across the reference planes are both sinusoidal,

$$\begin{cases} V_1 = \alpha_1 V_p \\ V_2 = \alpha_2 V_p \\ \cdot \\ \cdot \\ \cdot \\ V_m = \alpha_m V_p \end{cases} \qquad \begin{cases} I_1 = \alpha_1 I_p/m \\ I_2 = \alpha_2 I_p/m \\ \cdot \\ \cdot \\ \cdot \\ I_m = \alpha_m I_p/m \end{cases} \tag{19}$$

where

$$\alpha_i = \sin\left(\frac{2i - 1}{2m}\pi\right),$$

$$\begin{cases} V_{m+1} = \beta_1 V_q \\ V_{m+2} = \beta_2 V_q \\ \cdot \\ \cdot \\ \cdot \\ V_{m+n} = \beta_n V_q \end{cases} \qquad \begin{cases} I_{m+1} = \beta_1 I_q/n \\ I_{m+2} = \beta_2 I_q/n \\ \cdot \\ \cdot \\ \cdot \\ I_{m+n} = \beta_n I_q/n \end{cases} \tag{20}$$

[2] We may remove half of this assumption, i.e., the presence of the straight waveguide sections "inside" the reference planes, if we consider $(m - 1)$ and $(n - 1)$ higher order modes in the input and output waveguides, respectively. Then we may take into account the (probably) reactive waveguide impedances for those higher order modes, and again no longer need the reduction of the constraints performed to obtain (22) and (23).

where

$$\beta_i = \sin\left(\frac{2i-1}{2n}\pi\right).$$

Using the previous relations, we may rewrite (5) as

$$[U_{ij}]\begin{bmatrix}\alpha_1 V_p\\ \cdot\\ \cdot\\ \cdot\\ \alpha_m V_p\end{bmatrix}\Big\}m \quad \begin{bmatrix}\alpha_1 I_p/m\\ \cdot\\ \cdot\\ \cdot\\ \alpha_m I_p/m\end{bmatrix}\Big\}m$$

$$\begin{bmatrix}\beta_1 V_q\\ \cdot\\ \cdot\\ \cdot\\ \beta_n V_q\end{bmatrix}\Big\}n = [H_{ij}]\begin{bmatrix}\beta_1 I_q/n\\ \cdot\\ \cdot\\ \cdot\\ \beta_n I_q/n\end{bmatrix}\Big\}n \quad (21)$$

$$\begin{bmatrix}0\\ \cdot\\ \cdot\\ \cdot\\ 0\end{bmatrix}\Big\}M \quad \begin{bmatrix}I_{m+n+1}\\ \cdot\\ \cdot\\ \cdot\\ I_{m+n+M}\end{bmatrix}\Big\}M$$

Following the procedure described in the preceding section, we again define the following $(M+2)\times(M+2)$ matrices to decrease the number of constraints, as

$$[U'] = \left[\begin{array}{ccc|c} \sum_{i=1}^{m}\sum_{j=1}^{m}\alpha_j U_{ij} & \sum_{i=1}^{m}\sum_{j=m+1}^{m+n}\beta_{j-m}U_{ij} & & \sum_{i=1}^{m} U_{i(m+n+1)}\cdots \\ \sum_{i=m+1}^{m+n}\sum_{j=1}^{m}\alpha_j U_{ij} & \sum_{i=m+1}^{m+n}\sum_{j=m+1}^{m+n}\beta_{j-m}U_{ij} & & \sum_{i=m+1}^{m+n} U_{i(m+n+1)}\cdots \\ \hline \sum_{j=1}^{m}\alpha_j U_{(m+n+1)j} & \sum_{j=m+1}^{m+n}\beta_{j-m}U_{(m+n+1)j} & U_{m+n+1\,m+n+1} & \cdots \\ \vdots & \vdots & \vdots & \\ & & U_{m+n+M\,m+n+M} & \end{array}\right] \quad (22)$$

$$[H'] = \text{(similar to the above)}. \quad (23)$$

Using the previous matrices, we may rewrite (21) in a form identical to (9). The transfer parameters are also derived in the same way.

V. EXAMPLES OF NUMERICAL ANALYSIS

A. Short-Circuited Radial Line

To show the validity and accuracy of the proposed method of analysis, two examples of numerical analysis whose results can be compared with analytical solutions will first be described. The first example is of the coaxial-coupled type: a thin radial line terminated by a short-circuit wall as shown in Fig. 5.

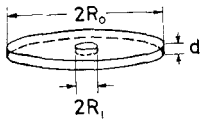

Fig. 5. A radial line.

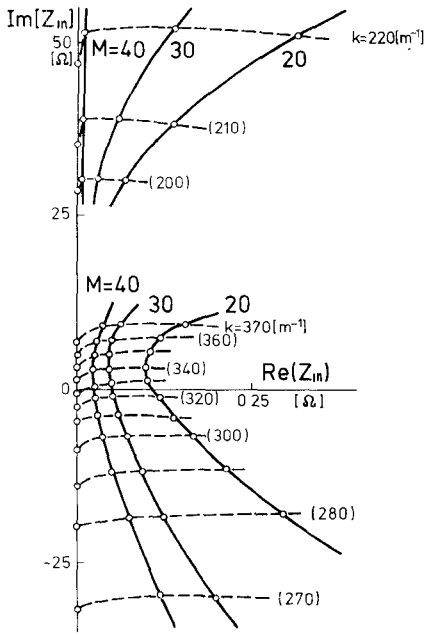

Fig. 6. The computed input impedance of a radial line. Note that the real part (abscissa) is exaggerated to show the computational error.

For such a one-port circuit, the driving-point impedance is given [1], instead of (16), by

$$-Z_p = B'/D'. \quad (24)$$

This driving-point impedance has been computed for dimensions (see Fig. 5) $R_i = 1$ mm, $R_o = 10$ mm, and $d = 0.5$ mm, at 21 frequencies ranging between $k(=2\pi f/c) = 200 \sim 400[\mathrm{m}^{-1}]$. Various numbers of divisions have been used to obtain the estimate of the computation error.

The results of the cases for $m = 10$ are shown in Fig. 6. The abscissa and the ordinate show the real and imaginary parts of the driving-point impedance, respectively. Note, however, that the abscissa is expanded by a factor of 100 to exaggerate the computation error. Small circles upon the ordinate show the theoretical values [3]

$$-Z_p = -j\frac{Z_{0i}d}{2\pi R_i}\frac{\sin(\theta_i-\theta_o)}{\cos(\varphi_i-\theta_o)} \quad (25)$$

where subscripts i and o represent the inner and outer boundaries, respectively, θ and φ are the quantities defined by

$$H_0^{(1)}(x) = J_0(x) + jN_0(x) = G_0(x)\exp(j\theta(x))$$

$$jH_1^{(1)}(x) = -N_1(x) + jJ_1(x) = G_1(x)\exp(j\varphi(x))$$

where $x = kr$, and Z_{0i} denotes the wave impedance at the inner boundary, defined as

$$Z_{0i} = 120\pi\{G_0(kR_i)/G_1(kR_i)\}[\Omega].$$

The bracketed numerals in Fig. 6 denote the wavenum-

ber in m^{-1}. Some of the broken curves (k = 200,210, 220[m^{-1}]) seem to converge for increasing M to values different from analytic ones. It is natural because m is finite.

The estimate of the error obtained from Fig. 6 is several-tenth ohms for the real part, and several ohms (in most cases below 2 Ω) for the imaginary part. The series resonance frequency obtained with the numerical analysis is 15.68 GHz (k = 328 m^{-1}) for m = 10, M = 40, which shows an error of approximately 1 percent as compared with the analytical value 15.87 GHz (k = 332 m^{-1}).

B. Uniform Waveguide Section

Another example, whose results can be compared with analytical ones, is a uniform waveguide section. A finite section of the standard X band rectangular waveguide with a (width) = 22.9 mm, b (height) = 10.2 mm, and l (length) = $2a$ = 45.8 mm is assumed to be terminated by a resistive sheet placed perpendicularly with respect to the waveguide axis; the surface resistance of the sheet is assumed to be equal to the waveguide impedance

$$Z_0 = 120\pi \frac{b}{a} \frac{1}{(1 - (\lambda/2a)^2)^{1/2}} [\Omega] \tag{26}$$

at f = 10.00 GHz (k = 209 m^{-1}), which is 222.2[Ω].

The results of the numerical computation of the driving-point impedance are shown in Fig. 7(a) with small dots, for $m = n$ = 10, M = 40. In the same figure, the theoretical value

$$Z_{in} = Z_0 \frac{(Z_L/Z_0) + j \tan (2\pi l/\lambda_g)}{1 + j(Z_L/Z_0) \tan (2\pi l/\lambda_g)} \tag{27}$$

is also plotted with small crosses where Z_L, Z_0, and λ_g denote the load impedance (222.2[Ω]), the waveguide impedance at the given frequency, and the wavelength in the guide, respectively. The complicated part (below, right) of Fig. 7(a) is shown in Fig. 7(b) in an enlarged scale.

C. Waveguide Section Including a Thick Inductive Window

In the following three subsections, more practical circuits are analyzed numerically; the obtained results are compared with the approximate analyses and experimental data. In those numerical analyses, for convenience of comparison, the obtained transfer parameters are once converted into equivalent T-circuit parameters; this conversion process will first be described.

We consider a waveguide section including a symmetrical obstacle, a thick inductive window as in the example shown in Fig. 8(a), and represent the entire section by three equivalent circuits: those of two straight sections and an equivalent T-circuit of the obstacle itself.

If we denote the transfer parameters of the entire section, the straight sections and the obstacle by F_c, F_L, and F_T, respectively,

$$[F_c] = [F_L][F_T][F_L]. \tag{28}$$

If the straight sections are lossless,

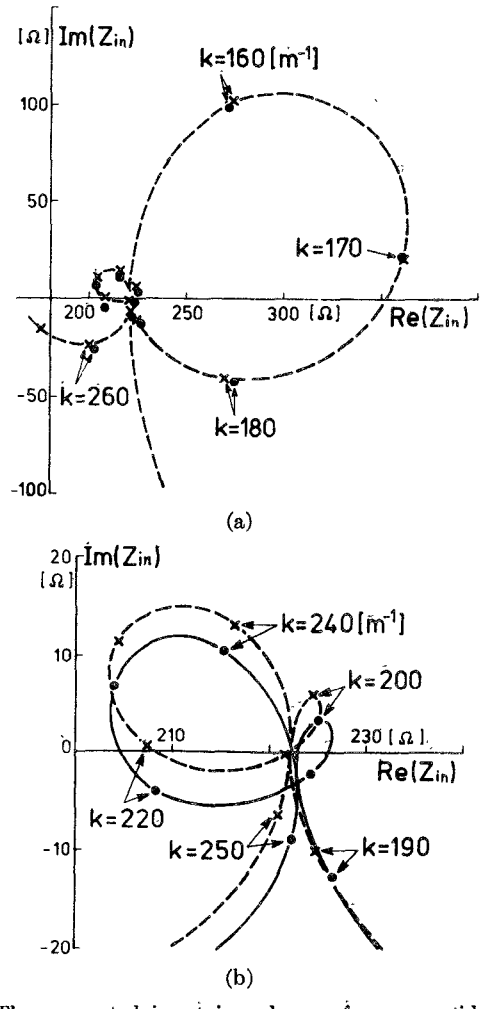

Fig. 7. The computed input impedance of a waveguide section. (a) The overall frequency characteristics. (b) An enlarged figure of a portion.

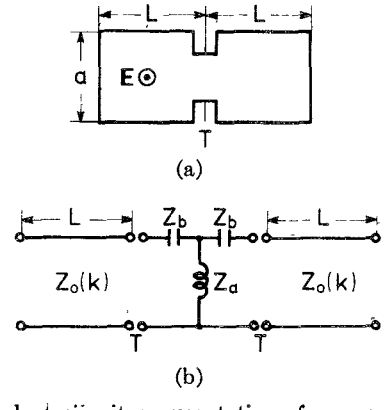

Fig. 8. Equivalent circuit representation of a symmetrical waveguide obstacle. (a) A thick inductive window (an example). (b) The equivalent T-circuit representation.

$$[F_L] = \begin{bmatrix} \cos\left(\frac{2\pi L}{\lambda_g}\right) & jZ_0 \sin\left(\frac{2\pi L}{\lambda_g}\right) \\ j\left(\frac{1}{Z_0}\right) \sin\left(\frac{2\pi L}{\lambda_g}\right) & \cos\left(\frac{2\pi L}{\lambda_g}\right) \end{bmatrix}. \tag{29}$$

From the elements of F_c computed numerically and those of F_L, the elements of F_T are obtained as

$$[F_T] = \begin{bmatrix} A_T & B_T \\ C_T & D_T \end{bmatrix} = [F_L]^{-1}[F_c][F_L]^{-1}. \quad (30)$$

On the other hand, F_T is expressed by the T-circuit parameters as

$$[F_T] = (1/Z_a) \begin{bmatrix} Z_a + Z_b & 2Z_aZ_b + Z_b^2 \\ 1 & Z_a + Z_b \end{bmatrix}. \quad (31)$$

Hence, the normalized T-circuit parameters are given in terms of the computed elements of F_T as

$$\frac{Z_a}{Z_0} = \frac{1}{C_T Z_0} \left(\triangleq j \frac{X_a}{Z_0} \right) \quad (32)$$

$$\frac{Z_b}{Z_0} = \frac{A_T - 1}{C_T Z_0} \left(\triangleq -j \frac{X_b}{Z_0} \right). \quad (33)$$

Fig. 9 shows the results of computer analyses of the frequency characteristics of thick inductive windows. The ordinate gives the normalized T-circuit parameters X_a/Z_0 and X_b/Z_0. The dimensions of the circuit are assumed to be

Case 1:

$a = 22.9$ mm $\quad d'/2 = 2.29$ mm $\quad l = 2.29$ mm

$L = 24.045$ mm

Case 2:

$a = 22.9$ mm $\quad d'/2 = 2.29$ mm $\quad l = 4.58$ mm

$L = 25.19$ mm.

The total sampling-point number is 66 in case 1, and 68 in case 2.

The dots in Fig. 9 show the results of the computer analyses. The crosses show the approximate theoretical values described in [4]. The difference between dots and crosses is found to be less than 0.02. (The errors in X_b/Z_0 might seem rather large; however, note that the scales of the ordinate for X_b/Z_0 and X_a/Z_0 are different.)

D. Waveguide Sections Including Corners

The dots in Fig. 10 show the results of the computer analyses of 30° and 60° waveguide corners. The ordinate again shows X_a/Z_0 and X_b/Z_0. The circuit dimensions are $a = 22.9$ mm and $L = 22.9$ mm, and the total sampling-point number $N = 66$ for $\alpha = 30°$ and $N = 72$ for $\alpha = 60°$. Small crosses in the figure show the experimental data found in [4].

E. Waveguide Sections Including Post

The dots in Fig. 11 show the results of the computer analyses of waveguide sections including post. The circuit dimensions are $a = 22.9$ mm and $L = 22.9$ mm, and the total sampling-point number $N = 72$, including 12 points around the post. Small crosses show the experimental data found in [4].

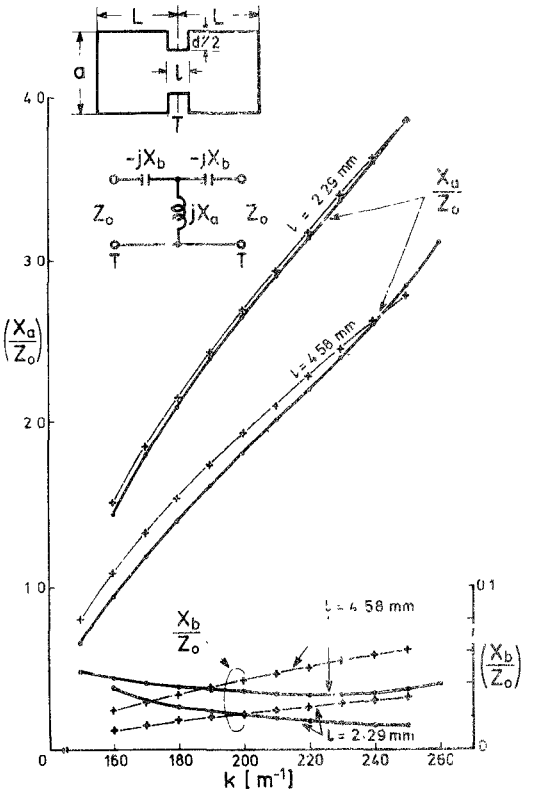

Fig. 9. The computed equivalent-circuit parameters of thick inductive windows. Crosses show the results of the approximate analysis described by Marcuvitz [4].

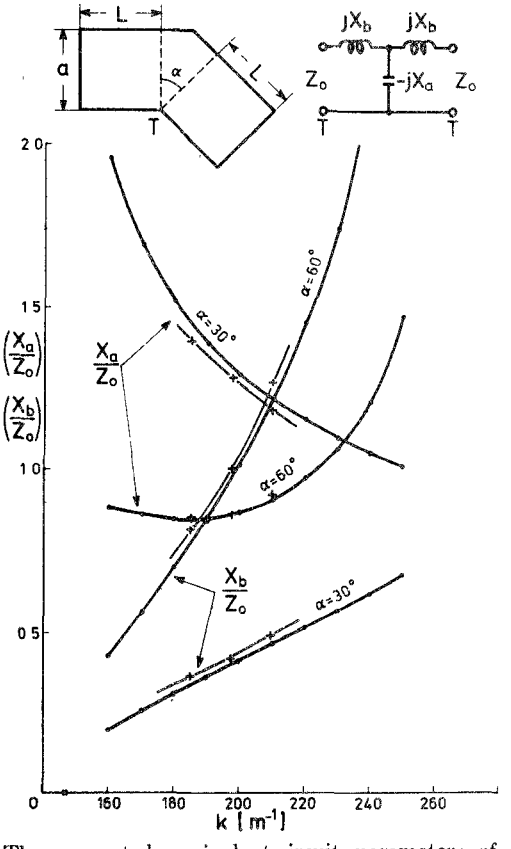

Fig. 10. The computed equivalent-circuit parameters of waveguide corners. Crosses show the experimental data described by Marcuvitz [4].

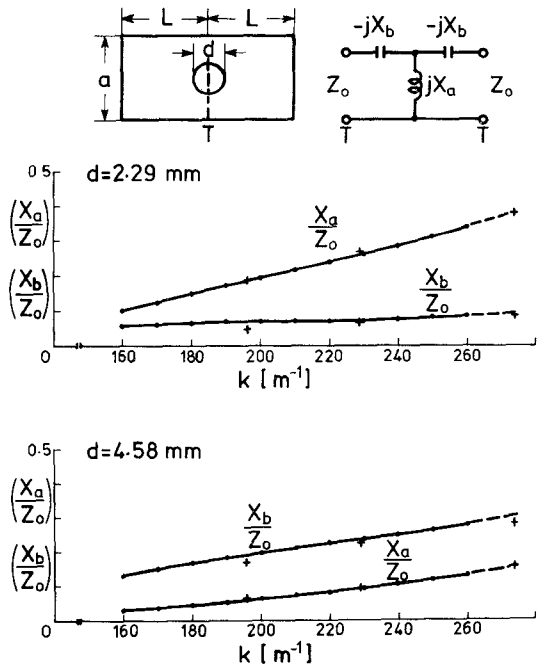

Fig. 11. The computed equivalent-circuit parameters of a post in a waveguide. Crosses show the results of the approximate analysis described by Marcuvitz [4].

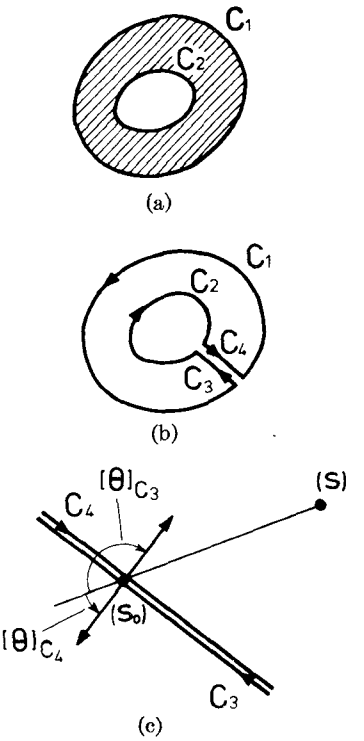

Fig. 12. Proof of (1) for a multiply connected planar circuit pattern.

VI. CONCLUSION

The basic program for the computer analysis of arbitrarily shaped, short-boundary planar circuits has been completed. The validity and error of the proposed method of analysis has been shown through comparison with theories. The required computer time is still long; for example, about 10 min are required to obtain all the dots in Fig. 9 using HITAC-8800, one of the standard Japanese high-speed computers. The improvement of the program toward shorter computer time and better accuracy is left for further efforts.

APPENDIX

PROOF OF (1) FOR A MULTIPLY CONNECTED CIRCUIT PATTERN

We now consider a planar circuit pattern having a hole as shown in Fig. 12(a). We connect the outer and inner boundaries, C_1 and C_2, with contours C_3 and C_4 which are infinitesimally separated, and give a direction of integration, as shown in Fig. 12(b), to define θ. For the entire contour $C_1 + C_2 + C_3 + C_4$, obviously (1) holds. However, for the corresponding points upon C_3 and C_4 [see Fig. 12(c)],

$$[V(s_0)]_{C3} = [V(s_0)]_{C4} \tag{34}$$

$$[i_n(s_0)]_{C3} = -[i_n(s_0)]_{C4} \tag{35}$$

must be satisfied.

The voltage $V(s)$ in the left-hand side of (1) in the text needs to be known only upon C_1 and C_2. If we consider cases in which s is located somewhere upon C_1 or C_2 and s_0 is located somewhere upon C_3 and C_4, we obtain for the corresponding points upon C_3 and C_4

$$[\theta]_{C3} = [\theta]_{C4} + \pi. \tag{36}$$

Hence,

$$[\cos\theta]_{C3} = -[\cos\theta]_{C4}. \tag{37}$$

Putting (34), (35), and (37) into the right-hand side of (1), we find that the integrals along C_3 and C_4 cancel each other. Hence, we may apply (1) to a pattern like Fig. 12(a) provided that the direction of integration along C_1 and C_2 be carefully defined.

ACKNOWLEDGMENT

The authors wish to thank S. Oda of Hitachi Ltd. for his help in the early stage of this work.

REFERENCES

[1] T. Okoshi and T. Miyoshi, "The planar circuit—An approach to microwave integrated circuitry," *IEEE Trans. Microwave Theory Tech.*, vol. MTT-20, pp. 245–252, Apr. 1972.
[2] J. A. Stratton, *Electromagnetic Theory.* New York: McGraw-Hill, 1941, p. 460.
[3] S. Ramo and J. R. Whinnery, *Fields and Waves in Modern Radio.* New York: Wiley, 1953.
[4] N. Marcuvitz, *Waveguide Handbook.* New York: McGraw-Hill, 1951.